Sliding Viscoelastic Contacts: Reciprocating Adhesive Contact Mechanics and Hysteretic Loss

Sliding viscoelastic contacts: Reciprocating adhesive contact mechanics and hysteretic loss

Guido Violano[1], Giuseppe Demelio[1], Luciano Afferrante[1*]

[1*]Department of Mechanics, Mathematics and Management, Polytechnic University of Bari, Via E. Orabona 4, Bari, 70125, Italy.

*Corresponding author(s). E-mail(s): luciano.afferrante@poliba.it; Contributing authors: guido.violano@poliba.it; giuseppepompeo.demelio@poliba.it;

Abstract

This study investigates the reciprocating motion of a rigid Hertzian indenter on a viscoelastic substrate with adhesion, using a finite element-based numerical model. An innovative methodology is employed to transform the sliding contact problem into an equivalent normal contact problem, enabling the accurate simulation of adhesion effects at the contact interface.

The results reveal that system behaviour is governed by the interplay between viscoelasticity and adhesion, leading to notable changes in contact pressure distribution, contact area, and energy dissipation during reciprocating motion. Specifically, viscous dissipation within the substrate material dominates at intermediate sliding speeds, where the interaction between adhesion and viscoelastic relaxation processes results in pronounced hysteresis cycles. In contrast, at low and high sliding speeds (corresponding to the rubbery and glassy regions, respectively), the material behaviour is predominantly elastic, and no hysteresis is observed.

Adhesion influences contact pressure distribution and contact size, particularly in the transition regime, where its effects on viscous dissipation are measurable. Moreover, the study clarifies that adhesion alone does not induce hysteresis in elastic regimes, distinguishing reciprocating contact from normal contact, where adhesive hysteresis is typically observed. New insights are also provided into how adhesion and viscoelasticity jointly impact tribological performance, offering a deeper understanding of energy dissipation mechanisms and contact mechanics during motion reversal.

Interestingly, our results also show that there is a lag period after motion reversal where friction aligns with motion direction before eventually changing direction as pressure redistribution occurs within the system. This phenomenon highlights how changes in contact mechanics affect local tribological interactions and can lead to variations in overall system response.

Keywords: Viscoelasticity, Finite Element Method, Energy loss, Friction coefficient, Reciprocating tangential contact

1 Introduction

Reciprocating tangential contact between a rigid indenter and a viscoelastic substrate is a topic of significant practical interest. This scenario arises in numerous engineering applications where the direction of motion periodically reverses. A prominent example at the macroscopic scale is the use of viscoelastic dampers in civil constructions. These devices exploit the hysteretic energy dissipation caused by the cyclic deformation of the bulk viscoelastic material to absorb the energy released during earthquake and wind induced motion [1, 2]. Cyclic motion is prevalent also in mechanical engineering applications where viscoelastic components are employed, like tires [3], seals [4, 5], and soft bearings [6]. Reciprocating contacts extend beyond the macroscopic world and are also observed at micro and nanoscales. Examples include microelectromechanical systems (MEMS) [7] where tiny components undergo repeated sliding motions, and even within biological systems at the cellular level [8].

For micro and nanoscale contacts [9] (when the contacting bodies have a high surface area-to-volume ratio) and/or for compliant soft materials [10] (like rubber and silicones), adhesion becomes a critical factor in contact mechanics. In these scenarios, the interplay between viscoelasticity and adhesion can significantly influence tangential motion [11]. This combined effect can impact the overall performance (e.g., efficiency, functionality) and durability (e.g., wear resistance, fatigue life) of adhesive systems [12, 13].

The first scientific studies explored the dynamics of sliding contacts without adhesion. For instance, Hunter [14] provided the first methodology to study the rolling contact of a cylinder with a viscoelastic material, highlighting the importance of considering time-dependent material properties, particularly in systems subjected to repetitive loading and unloading cycles. Even before the work of Hunter, Tabor [15] intuited that interfacial micro-slip related to the coulomb friction component are only partially responsible of the rolling friction, identifying the hysteresis losses in the bulk of material as the main reason for rolling resistance. After, Goriacheva [16] proposed a theoretical model to investigate the 1D+1D rolling between viscoelastic bodies, based on the identification of two zones in the contact length: the sticking and slipping zones. Further recent studies (see, for example, [17–19]), have highlighted the crucial role of material dissipation in originating rolling resistance.

However, in such studies it is not simple distinguishing the contribution of the material dissipation from that of the Coulomb friction. For this reason, many recent studies have addressed the problem by neglecting Coulomb friction at the interface. For example, Menga at al. [20, 21] investigated the sliding contact between a rigid sinusoidal surface and a viscoelastic substrate, finding that a transition from full contact to partial contact can occur depending on the sliding velocity and remote applied load. This is due to the viscoelastic stiffening of the material and the periodicity of the contacts.

Putignano et al. [22] and Afferrante et al. [23] demonstrated, through numerical and theoretical models, that viscoelasticity induces also anisotropy in contact of rough surfaces. Additionally, the non-symmetric distribution of the normal contact pressure results in a force perpendicular to the sliding direction, which, however, does not dissipate energy.

Recent studies have utilized numerical methods to simulate the effects of viscoelasticity in reciprocating sliding contacts. For example, Putignano et al. [24], and Putignano and Carbone [25, 26] have demonstrated that the contact area is significantly influenced by the indenter's position and by the speed, with tangential forces exhibiting a complex hysteretic cycle. The roughness scales play a crucial role in viscoelastic dissipation. Similarly, Putignano [27] has provided insights into the periodic nature of viscoelastic contacts, elucidating that for reciprocating sliding of a sinusoidal punch on a viscoelastic surface, sliding velocity influences energy dissipation, and high velocities can lead to loss of contact during the return phase.

The aforementioned studies have focused on sliding/reciprocating contact without considering interfacial adhesion. However, macroscopic adhesion is frequently observed in soft materials [28–30]. Grosch [31], through his experiments conducted in 1963, already hypothesized the importance of adhesion in addition to the deformation losses. In soft contacts, compliant materials like rubber and silicones may exhibit short-range adhesion. This type of adhesion is characterized by strong interactions confined within the contact area, leading to significant deformation of the contacting surfaces [10]. In contrast, stiff materials exhibit long-range adhesion [32], as seen in micro-electromechanical systems (MEMS) [9]. Here, adhesive forces act beyond the immediate contact region, with the primary source of deformation arising from the repulsive component of interfacial pressure [33, 34]. In the framework of Hertzian contacts, the transition between long-range and short-range adhesion is governed by the so-called Tabor parameter [35], which depends on geometrical and material properties.

Recent studies have primarily focused on normal adhesive contact [11, 36–39], where viscoelasticity introduces rate effects leading to an "effective surface energy". Afferrante & Violano [37] demonstrated that this energy, representing the work required to separate the bodies, monotonically increases with contact line speed for initially relaxed materials. However, for unrelaxed materials, the effective surface energy exhibits a maximum at intermediate contact line velocities, highlighting a transition zone dominated by viscous dissipation.

Despite boundary element method (BEM) based approaches have been developed to study tangential adhesive contacts under steady-state sliding [11, 40, 41], no research has investigated reciprocating tangential contact with both adhesion and viscoelasticity. This gap in knowledge represents an opportunity for further exploration.

Building upon our prior work [42], which introduced a novel Finite Element (FE) method for simulating the adhesive tangential contact of a rigid indenter on a viscoelastic substrate, this study explores reciprocating contact with adhesion. Our results demonstrate that both adhesion and viscoelasticity play a role in governing the system's behaviour. However, interestingly, only viscoelasticity contributes to energy dissipation within a reciprocating cycle. Notably, upon reversal of motion, the friction force initially aligns with the new sliding direction until the interfacial pressure redistributes within the contact region.

2 Formulation

To simulate the line contact problem of a Hertzian rigid profile in reciprocating motion on a viscoelastic substrate, we adopt the numerical model developed in Ref. [42], where the sliding contact in presence of adhesion is solved with the aid of the finite element-based methodology originally developed by Afferrante and Violano [37]. The geometry of the problem is illustrated in Fig. 1a.

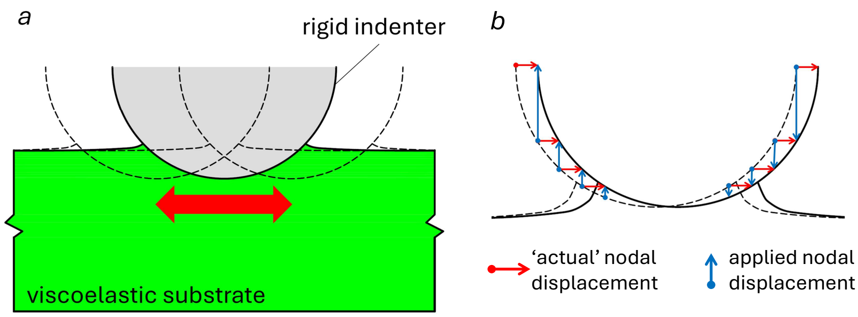

Fig. 1 a) A rigid Hertzian indenter of radius R is in reciprocating tangential contact with a viscoelastic substrate at fixed sliding speed. b) A schematical representation of the methodology adopted to move horizontally the rigid indenter. The tangential displacement is simulated by moving the nodes of the indenter in the vertical direction. Red arrows denote the tangential uniform displacement of the indenter nodes, which is generated by moving the nodes in vertical direction consistently with the blue arrows shown in the picture.

The substrate material is modelled using a standard linear solid model with one relaxation time, $\tau = 10^{-4}s$, and a ratio of low- to high-frequency modulus, $E_0/E_\infty = 0.1$. The relaxation function is derived based on the Maxwell scheme representation [43], which consists of a spring (E_0) in parallel with a dashpot ($(E_0 - E_\infty)/\tau$), both arranged in series with another spring ($E_0 - E_\infty$). This representation describes the frequency-dependent behaviour of the modulus, characterized by a transition from the low-frequency modulus (E_0) to the high-frequency modulus (E_∞) as the frequency (ω) increases. Specifically, the dynamic modulus $E(\omega)$ in the Maxwell model evolves with the frequency as

$$E(\omega) = E_\infty + \frac{E_0 - E_\infty}{1 + i(\omega\tau)} \tag{1}$$

where i is the imaginary unit. This relationship and its implications for the material response are well-documented in the literature, as discussed, for example, in Ref. [37].

Surface interactions are instead modelled using Derjaguin's approximation [44], applying a traction-gap relationship derived from the Lennard-Jones potential,

$$p_{\mathrm{LJ}} = \frac{8\Delta\gamma}{3\epsilon}\left[\left(\frac{\epsilon}{g}\right)^3 - \left(\frac{\epsilon}{g}\right)^9\right] \tag{2}$$

where g is the local separation between the surfaces, ϵ is the equilibrium distance under zero applied load [45], and $\Delta\gamma$ is the surface energy of adhesion.

As described in Ref. [42], the problem is solved first approaching the rigid indenter to the substrate up to a fixed penetration δ. Then, the substrate is subjected to the total force generated at the end of the vertical approach and its nodes are conveniently moved in vertical direction to simulate the interfacial sliding (see Fig. 1b). Once steady state is reached, the motion is periodically reversed, as shown in Fig. 1a. In our simulations, we have deliberately assumed quasi-static solutions, neglecting inertial effects and dynamic adhesion processes. The quasi-static assumption implies that the system is in equilibrium at each time step, and the rate of change of adhesion forces is sufficiently slow to allow the system to adapt instantaneously to changes in external conditions. As a result, phenomena such as the time-dependent formation and rupture of molecular junctions, or inertia-induced deviations from equilibrium, are not explicitly included in the model. The quasi-static approach allows us to isolate the effects of adhesion and viscoelasticity without introducing additional complexities from dynamic processes, allowing to capture the primary interactions between adhesion and the viscoelastic substrate. Furthermore, we have assumed a constant sliding speed during reciprocating motion. The velocity reverses its sign at the motion reversal, with the reversal occurring over a time interval $t = \Delta x/V_s$, where Δx is the element size and V_s is the magnitude of the speed. While it is possible to consider alternative time evolutions for the velocity, such as a sinusoidal variation, we expect that this would not significantly alter the results under the quasi-static motion assumption.

3 Results

Results are presented with the aim of highlighting the interplay between adhesion and viscoelastic dissipation in the substrate. For this reason, simulations are performed for different values of the Tabor parameter $\mu_T = (R\Delta\gamma^2/E_0^{*2}\epsilon^3)^{1/3}$ (with $E_0^* = E_0/(1-\nu^2)$ the plain strain elastic modulus), ranging from long-range adhesion regime ($\mu_T < 1$) to short-range adhesion regime ($\mu_T > 3$). Moreover, calculations are performed on a nearly incompressible material (Poisson's ratio $\nu = 0.49$) with a ratio of low to high-frequency modulus $E_0/E_\infty = 0.1$.

Results are presented in terms of the following dimensionless quantities: sliding speed $\hat{V}_s = V_s\tau/\epsilon$, contact force $\hat{F} = F/(E_0^* R)$, time $\hat{t} = t/\tau$, dissipated energy $\hat{W} = W/(E_0^* R l_0)$, where l_0 is the amplitude of the reciprocating motion, and pressure $\hat{p} = p/\sigma_{\max}$, being $\sigma_{\max} = 16\Delta\gamma/(9\sqrt{3}\epsilon)$ the Lennard-Jones tensile peak stress.

It is well known that viscoelastic materials exhibit a frequency-dependent response. At low and high frequencies (speeds), the material response is essentially elastic with moduli E_0 (rubbery region) and E_∞ (glassy region), respectively. At intermediate frequencies (speeds), viscous effects are activated, leading to energy dissipation (transition region). As a result, after the inversion of the motion, we expect the substrate response to depend on the tangential speed, as the excitation frequency is directly correlated with V_s. This behaviour influences the contact pressure, as illustrated in Figs. 2 and 3, where the pressure distribution $\hat{p} = p/\sigma_{max}$ is shown at different instants after the reversal of the motion, which occurs at $\hat{t} = t/\tau = 0$, for two values of the Tabor parameter $\mu_T = 1$ and $\mu_T = 6.08$, respectively.

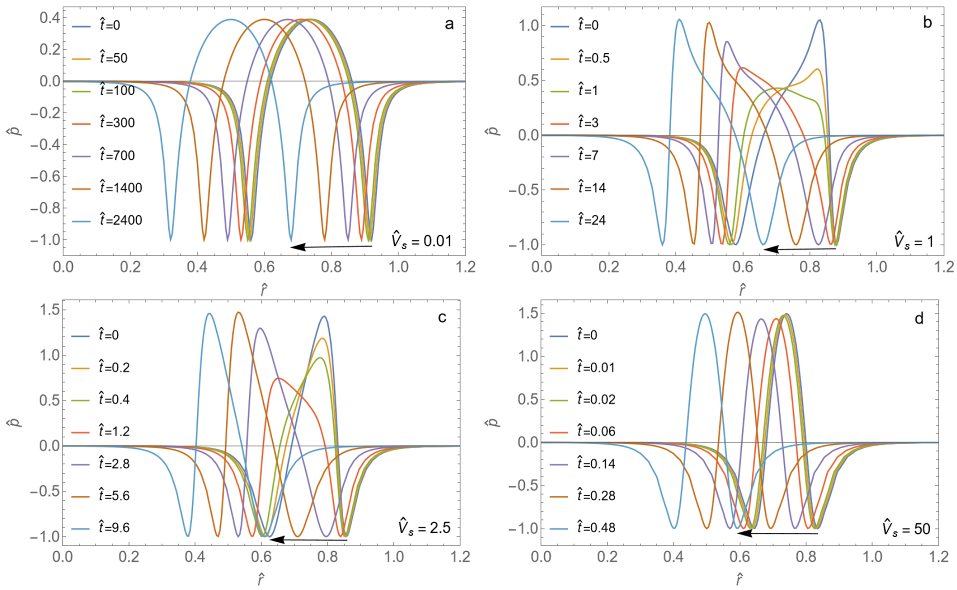

Fig. 2 The adimensional pressure distribution $\hat{p}$, in the contact region at different times after the motion reversal. Figures correspond to different values of the adimensional sliding speed $\hat{V}_s = V_s\tau/\epsilon$. Results are obtained under force-controlled conditions ($\hat{F}_n = -0.0047$), Tabor parameter $\mu_T = 1$, and $E_0/E_\infty = 0.1$. Black arrows indicate the direction of motion and the distance required to have a complete inversion of the pressure profile.

At low and high speeds, the material response is elastic, both in long-range (Fig. 2) and short-range (Fig. 3) adhesion regime. The pressure profiles are symmetric (Figs. 2a and 3a and Figs. 2d and 3d) and, after the motion reversal, neither the pressure shape nor the contact length changes.

At intermediate speeds, the behaviour changes significantly due to the viscoelastic dissipation within the substrate material, resulting in an asymmetric pressure profile. Specifically, at $\hat{t} = 0$, there are tensile (negative) peaks at the trailing and leading edges. However, near the leading edge, a compressive (positive) pressure peak is also present. After the reversal of the motion, as the leading and trailing edges switch positions, the contact pressure redistributes (Figs. 2b and 3b and Figs. 2c and 3c). The asymmetry in the contact pressure observed in the transition region, is characterized by the presence of a compressive peak, due to the viscoelastic time delay that prevents the material to completely relaxing. When the motion reverses, the compressive peak gradually reduces until it disappears, and a new compressive peak emerges at the opposite edge.

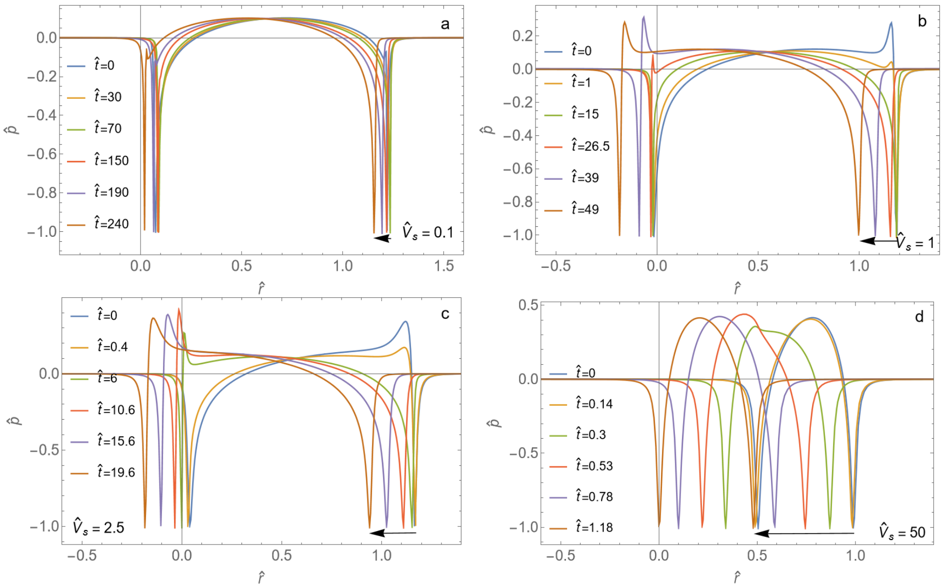

Fig. 3 The adimensional pressure distribution $\hat{p}$, in the contact region at different times after the motion reversal. Figures correspond to different values of the adimensional sliding speed $\hat{V}_s = V_s \tau / \epsilon$. Results are obtained under force-controlled conditions ($\hat{F}_n = 0.012$), Tabor parameter $\mu_T = 6.08$, and $E_0/E_\infty = 0.1$. Black arrows indicate the direction of motion and the distance required to have a complete inversion of the pressure profile.

Note that, in the short-range adhesion regime (Fig. 3), the extent of the zone required for a complete inversion of the pressure profile is significantly influenced by the sliding speed and increases with it. Additionally, the pressure tensile peaks are sharper.

The definition of the contact length $\mathcal{L}$ is nontrivial when the surface interactions are modelled with cohesive laws. However, based on results by Greenwood [46] and Feng [47, 48], and the discussion reported in Ref. [42], the contact region can be identified as the region where the gap is nearly constant, and the pressure peaks near the edges, at least when the Tabor parameter $\mu_T > 0.1$. Thus, we can define a gap threshold below which the points are considered to be in contact. This threshold is assumed 20% lager than the equilibrium distance ϵ.

The transition phase causes local variations in the contact length $\mathcal{L}$, as shown in Fig. 4, where the ratio of $\mathcal{L}$ to its steady state value $\mathcal{L}_0$ is plotted against the adimensional abscissa $\hat{r} = r/R$, indicating the indenter position during a complete cycle of the alternating motion. Curves are given for different sliding speeds.

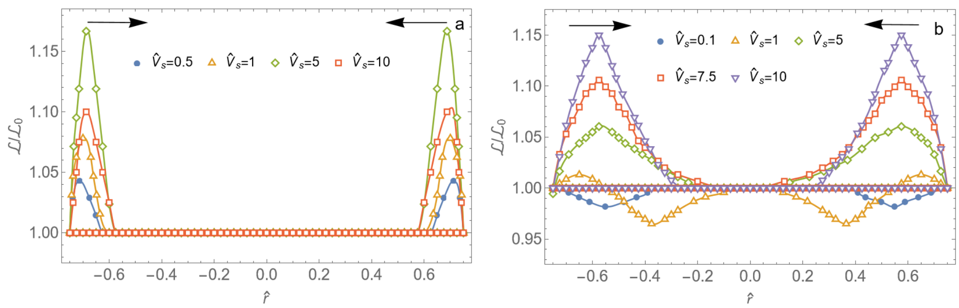

Fig. 4 The normalized contact length $\mathcal{L}/\mathcal{L}_0$ as a function of the indenter position during a complete cycle of alternating motion, for different values of the adimensional sliding speed $\hat{V}_s = V_s\tau/\epsilon$, and (a) long-range adhesion regime ($\mu_T = 1$) and (b) short-range adhesion regime ($\mu_T = 6.08$). Results are obtained under force-controlled conditions ($\hat{F}_n = -0.0026$ for $\mu_T = 1$ and $\hat{F}_n = -0.009$ for $\mu_T = 6.08$) and $E_0/E_\infty = 0.1$. Black arrows indicate the directions of motion.

In the long-range adhesion regime (Fig. 4a), after each motion reversal, the contact size sharply increases, reaches a maximum, and then returns to its steady state value. For $\hat{V}_s > 5$, the variation in $\mathcal{L}$ during the transition phase progressively reduces and vanishes as the sliding speed exceeds $\hat{V}_s > 50$.

In the short-range adhesion regime (Fig. 4b), the behaviour of the contact length $\mathcal{L}$ is more complex. After the motion reversal, the contact length can oscillate depending on the sliding speeds. Specifically, at low speeds, the motion reversal is accompanied by an initial reduction in contact length. As the speed increases, we observe an initial growth of $\mathcal{L}$, followed by a reduction and a subsequent increase to the steady state value. At higher speeds, after the punch reverses its motion, a local increase is always detected. In all cases, after a certain interval depending on $\hat{V}_s$, the steady-state value is eventually recovered.

The asymmetric pressure distribution leads to a viscoelastic friction force [49, 50]

$$F_t = -\int_{\mathcal{L}} p(x)\frac{\partial u}{\partial x}dx, \tag{3}$$

where u is the normal displacement at the contact interface.

The observed increase in the contact length is accompanied to a local increase in dissipation and, consequently, viscoelastic friction, as shown in Fig. 5. Under the assumptions of the present work (frictionless and adhesive interface, uncoupled normal and tangential displacements, viscoelastic material, and sliding at fixed normal force), this initial increase is related to the redistribution of contact pressure occurring in this phase, which also causes the friction to initially align with the sliding direction, as shown below.

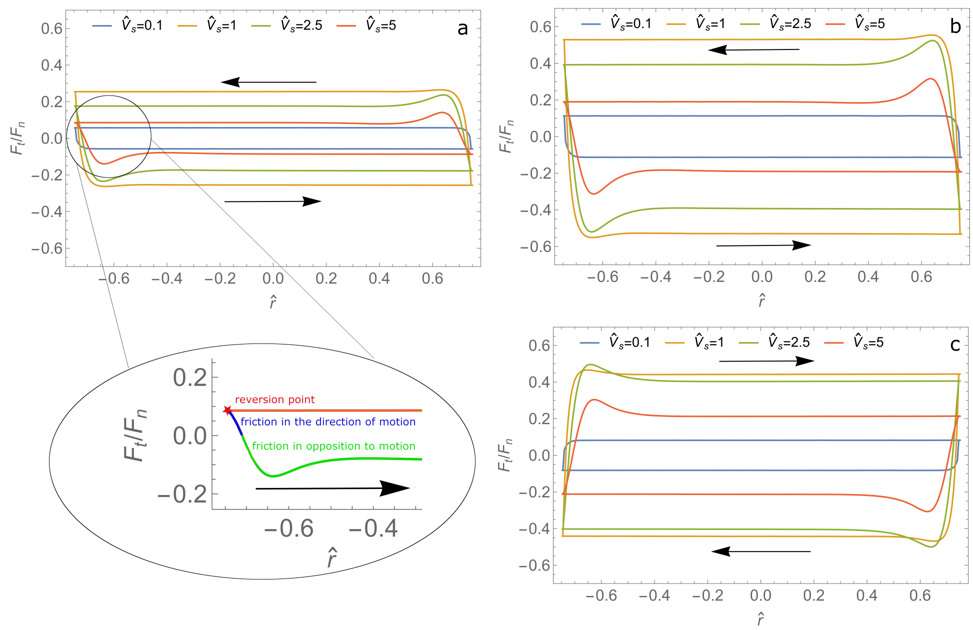

Fig. 5 The ratio F_t/F_n between the tangential (friction) and normal force during a complete cycle of the alternating motion, for different values of the adimensional sliding speed $\hat{V}_s = V_s\tau/\epsilon$ and at three different normal load: (a) $\hat{F}_n = -0.0047$, (b) $\hat{F}_n = -0.0026$, (c) $\hat{F}_n = 0.0042$. Results are obtained for Tabor parameter $\mu_T = 1$, and $E_0/E_\infty = 0.1$. Black arrows indicate the directions of motion.

In the rubbery and glassy regions (low and high speeds, respectively), where the material behaviour is elastic and the effects of viscous dissipation are negligible, no hysteresis is observed. In these regions, the contact pressure distribution remains symmetric during motion reversal, leading to no additional dissipation. Therefore, an important distinction can be observed between reciprocating and normal contact. In reciprocating contact, adhesion does not induce hysteresis in elastic regimes because the pressure distribution remains symmetric during motion reversal.This behavior is fundamentally different from normal contact, where adhesion, even in elastic regimes, causes differences between the loading and unloading paths due to jump-in and jump-out instabilities, a phenomenon commonly referred to as adhesive hysteresis.

In the transition region of intermediate sliding speeds, adhesion significantly alters the contact pressure distribution compared to the non-adhesive case, and friction exhibits a clear hysteresis cycle, with amplitude dependent on sliding velocity. Near the dead points, where the motion reverses, friction F_t/F_n aligns with the sliding speed, as illustrated in the zoom from Fig. 5a (see also Putignano et al. [24], for the case without adhesion). The extent of the region where the friction aligns with the motion direction slightly increases with speed, even after the hysteresis cycle starts to diminish. This result is consistent with the contact pressure behaviour observed in Fig. 2. After the inversion of the motion, the pressure needs finite time to redistribute according to the new direction. During this period, friction maintains the same direction until pressure redistribution causes a change. Finally, note that the hysteresis cycle direction changes when the total normal force becomes compressive (Fig. 5c), and the extent of hysteresis is significantly affected by sliding speed and normal load applied to the system.

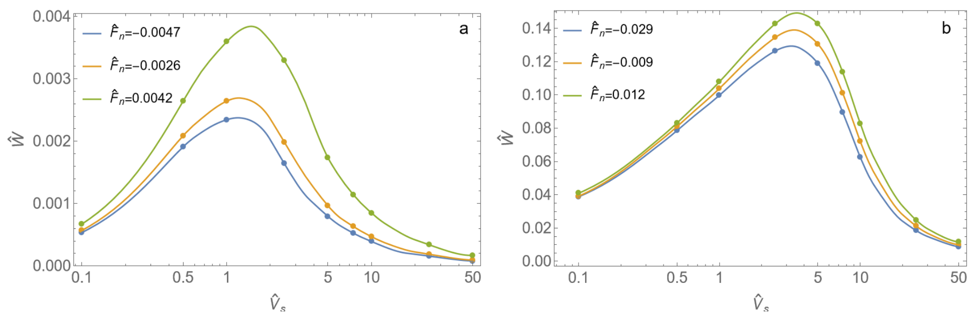

Fig. 6 The adimensional energy $\hat{W}$ dissipated during a reciprocating cycle as a function of the adimensional speed $\hat{V}_s$, for different values of the total normal force $\hat{F}_n$, and (a) long-range adhesion regime ($\mu_T = 1$) and (b) short-range adhesion regime ($\mu_T = 6.08$). Curves are shown in a semi-logarithmic plot and are given for $E_0/E_\infty = 0.1$.

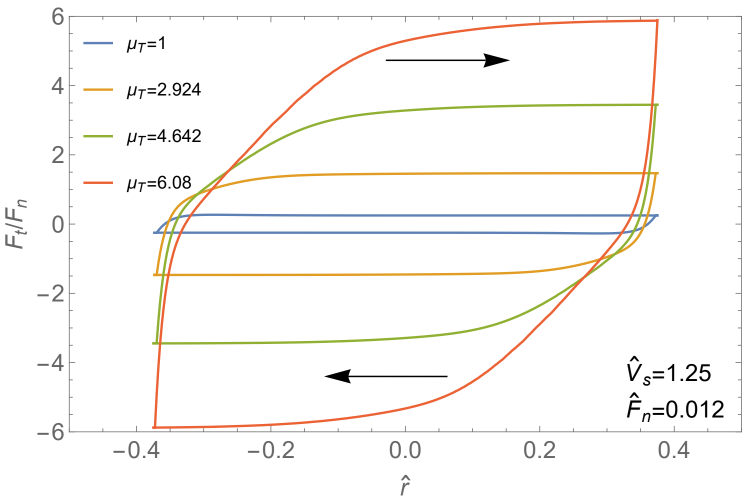

Fig. 7 The ratio F_t/F_n between the tangential (friction) and normal force during a complete cycle of the alternating motion, for different values of the Tabor parameter μ_T. Results are obtained for adimensional sliding speed $\hat{V}_s = 1.25$, normal force $\hat{F}_n = 0.012$, and $E_0/E_\infty = 0.1$. Black arrows indicate the directions of motion.

The energy dissipated in a single reciprocating cycle is shown in Fig. 6 as a function of sliding speed and for different values of the normal force. The results are presented in a semi-logarithmic chart for both the long-range (Fig. 6a) and short-range (Fig. 6b) cases. Moving from tensile to compressive force, the energy dissipated in a hysteresis cycle increases. Consistent with the plots in Fig. 5, viscous dissipation shows a peak at intermediate velocities and tends to vanish in the elastic limits (at low and high speeds).

In the short-range case, the dissipated energy exhibits a marked increase. Although the presence of interfacial adhesive interactions does not induce hysteresis in elastic regimes, as the contact pressure distribution remains symmetric during motion reversal, in the transition region, where viscoelastic effects cause an asymmetry in the contact pressure, adhesion further amplifies this asymmetry compared to the non-adhesive case. This results in increased hysteresis, as shown in Fig. 7, which displays the ratio F_t/F_n between the tangential (friction) and normal force during a complete cycle of the alternating motion for different values of the Tabor parameter μ_T.

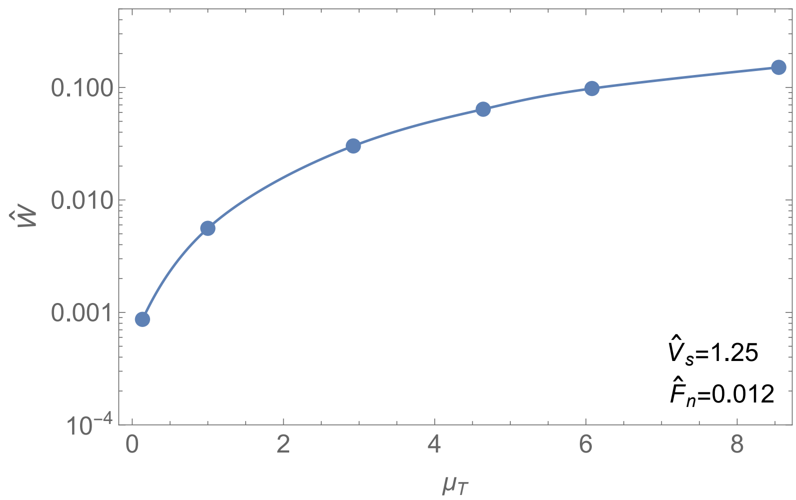

Fig. 8 The adimensional energy $\hat{W}$ dissipated during a reciprocating cycle as a function of the Tabor parameter μ_T. Curves are presented in a semi-logarithmic plot and are shown for adimensional sliding speed $\hat{V}_s = 1.25$, normal force $\hat{F}_n = 0.012$, and $E_0/E_\infty = 0.1$.

The corresponding dissipated energy $\hat{W}$ is plotted against μ_T in Fig. 8 using a semi-logarithmic chart. The results clearly show that $\hat{W}$ increases as the intensity of the interfacial adhesive interactions becomes stronger. This indicates that adhesive interactions paly a pivotal role in amplifying the hysteresis cycle, leading to greater viscous dissipation within the viscoelastic substrate. This amplifiation effect is notable in the intermediate sliding speed regime, where the interplay between adhesion and viscoelastic relaxation processes alters the contact pressure distribution. At higher values of μ_T, the system moves to behaviour dominated by stronger adhesive forces, which enhance energy dissipation compared to cases with weaker or negligible adhesion. These findings highlight the critical role of adhesion as a parameter for tuning energy dissipation in viscoelastic systems subjected to reciprocating motion.

4 Conclusions

Our study highlights the importance of considering both viscoelasticity and adhesion effects when analyzing reciprocating contacts on viscoelastic substrates, emphasizing the factors governing hysteresis and energy dissipation. Our findings demonstrate that, for given material properties, the hysteresis cycle and the resulting viscous dissipation are primarily influenced by the adhesion parameter, the normal force, and the sliding speed. Specifically, the adhesion parameter significantly affects the contact pressure distribution, contact size, and energy dissipation. The normal force determines the overall contact area and pressure distribution, directly influencing the mechanical response during reciprocating motion. Finally, the sliding speed governs the transition between elastic-dominated and viscous-dominated regimes, with intermediate speeds producing the largest hysteresis loops and the highest energy dissipation due to the interplay between adhesion and viscoelastic relaxation processes. These results illustrate how adhesion modifies the contact behaviour, particularly in the intermediate sliding speed regime, where the interplay between adhesive forces and viscoelastic relaxation processes results in increased hysteresis and dissipation. Additionally, while adhesion alone does not induce hysteresis in elastic regimes at low and high sliding speeds (corresponding to rubbery and glassy states, respectively), it plays a crucial role in shaping the tribological response in transition regimes.

These findings hold significant implications in tribological reciprocating contacts between viscoelastic materials. By accounting for both viscoelasticity and adhesion, we can develop more accurate models and optimize material selection for improved wear resistance and reduced energy losses.

Acknowledgements

This work was partly supported by the Italian Ministry of University and Research under the Programme “Department of Excellence” Legge 232/2016 (Grant No. CUP - D93C23000100001) and by the European Union - NextGenerationEU through the Italian Ministry of University and Research under the programs: PRIN2022 (Projects of Relevant National Interest) grant nr. 2022SJ8HTC - ELectroactive gripper For mIcro-object maNipulation (ELFIN); PRIN2022 PNRR (Projects of Relevant National Interest) grant nr. P2022MAZHX - TRibological modellIng for sustainaBle design Of induStrial friCtiOnal inteRfacEs (TRIBOSCORE).

References

[1] Samali, B., Kwok, K.: Use of viscoelastic dampers in reducing wind-and earthquake-induced motion of building structures. Engineering Structures **17**(9), 639–654 (1995)

[2] Menga, N., Foti, D., Carbone, G.: Viscoelastic frictional properties of rubber-layer roller bearings (rlrb) seismic isolators. Meccanica **52**, 2807–2817 (2017)

[3] Lorenz, B., Oh, Y., Nam, S., Jeon, S., Persson, B.: Rubber friction on road surfaces: Experiment and theory for low sliding speeds. The Journal of chemical physics **142**(19) (2015)

[4] Thatte, A., Salant, R.F.: Effects of multi-scale viscoelasticity of polymers on high-pressure, high-frequency sealing dynamics. Tribology international **52**, 75–86 (2012)

[5] Mnif, R., Ben Jemaa, M., Kacem, N.H., Elleuch, R.: Impact of viscoelasticity on the tribological behavior of ptfe composites for valve seals application. Tribology transactions **56**(5), 879–886 (2013)

[6] Santeramo, M., Putignano, C., Vorlaufer, G., Krenn, S., Carbone, G.: On the role of viscoelasticity in polymer rolling element bearings: Load distribution and hysteretic losses. Mechanism and Machine Theory **189**, 105421 (2023)

[7] Beake, B.D., Harris, A.J., Liskiewicz, T.W., Wagner, J., McMaster, S.J., Goodes, S.R., Neville, A., Zhang, L.: Friction and electrical contact resistance in reciprocating nano-scale wear testing of metallic materials. Wear **474**, 203866 (2021)

[8] Angelini, T., Dunn, A., Urueña, J., Dickrell, D., Burris, D., Sawyer, W.: Cell friction. Faraday Discussions **156**(1), 31–39 (2012)

[9] Zhao, Y.-P., Wang, L., Yu, T.: Mechanics of adhesion in mems—a review. Journal of Adhesion Science and Technology **17**(4), 519–546 (2003)

[10] Violano, G., Chateauminois, A., Afferrante, L.: Rate-dependent adhesion of viscoelastic contacts, part i: Contact area and contact line velocity within model randomly rough surfaces. Mechanics of Materials **160**, 103926 (2021)

[11] Carbone, G., Mandriota, C., Menga, N.: Theory of viscoelastic adhesion and friction. Extreme Mechanics Letters **56**, 101877 (2022)

[12] Chang, E.P.: Viscoelastic properties of pressure-sensitive adhesives. The Journal of Adhesion **60**(1-4), 233–248 (1997)

[13] Possart, W., Brede, M.: Adhesive Joints: Ageing and Durability of Epoxies and Polyurethanes. John Wiley&Sons, ??? (2019)

[14] Hunter, S.: The rolling contact of a rigid cylinder with a viscoelastic half space **28(8)**, 611–617 (1961)

[15] Tabor, D.: The mechanism of rolling friction. The London, Edinburgh, and Dublin Philosophical Magazine and Journal Science **45(369)**, 1081–1084 (1954)

[16] Goriacheva, G.: Contact problem of rolling of a viscoelastic cylinder on a base of the same material. J. Appl. Math. Mech. **37(5)**, 925–933 (1973)

[17] Olaru, D.N., Stamate, C., Prisacaru, G.: Rolling friction in a micro tribosystem. Tribol. Lett. **35**, 205–210 (2009)

[18] Harrass, M., Friedrich, K., Almajid, A.A.: Tribological behavior of selected engineering polymers under rolling contact. Tribol. Int. **45**, 635–646 (2010)

[19] Lorenz, B., Persson, B.N.J., Dieluweit, S., Tada, T.: Rubber friction: comparison of theory with experiment. Eur. Phys. J. E. **34**, 129 (2011)

[20] Menga, N., Putignano, C., Carbone, G., Demelio, G.: The sliding contact of a rigid wavy surface with a viscoelastic half-space. Proceedings of the Royal Society A: Mathematical, Physical and Engineering Sciences **470**(2169), 20140392 (2014)

[21] Menga, N., Afferrante, L., Demelio, G., Carbone, G.: Rough contact of sliding viscoelastic layers: numerical calculations and theoretical predictions. Tribology International **122**, 67–75 (2018)

[22] Putignano, C., Menga, N., Afferrante, L., Carbone, G.: Viscoelasticity induces anisotropy in contacts of rough solids. Journal of the Mechanics and Physics of Solids **129**, 147–159 (2019)

[23] Afferrante, L., Putignano, C., Menga, N., Carbone, G.: Friction in rough contacts of linear viscoelastic surfaces with anisotropic statistical properties. The European Physical Journal E **42**, 1–8 (2019)

[24] Putignano, C., Carbone, G., Dini, D.: Theory of reciprocating contact for viscoelastic solids. Physical Review E **93**(4), 043003 (2016)

[25] Putignano, C., Carbone, G.: Viscoelastic damping in alternate reciprocating contacts. Scientific Reports **7**(1), 8333 (2017)

[26] Putignano, C., Carbone, G.: Viscoelastic reciprocating contacts in presence of finite rough interfaces: A numerical investigation. Journal of the Mechanics and Physics of Solids **114**, 185–193 (2018)

[27] Putignano, C.: Oscillating viscoelastic periodic contacts: A numerical approach. International Journal of Mechanical Sciences **208**, 106663 (2021)

[28] Gent, A.: Adhesion and strength of viscoelastic solids. is there a relationship between adhesion and bulk properties? Langmuir **12**(19), 4492–4496 (1996)

[29] Lorenz, B., Krick, B., Mulakaluri, N., Smolyakova, M., Dieluweit, S., Sawyer, W., Persson, B.: Adhesion: role of bulk viscoelasticity and surface roughness. Journal of Physics: Condensed Matter **25**(22), 225004 (2013)

[30] Tiwari, A., Dorogin, L., Bennett, A., Schulze, K., Sawyer, W., Tahir, M., Heinrich, G., Persson, B.: The effect of surface roughness and viscoelasticity on rubber adhesion. Soft matter **13**(19), 3602–3621 (2017)

[31] Grosch, K.A.: The relation between the friction and visco-elastic properties of rubber. Proc. R. Soc. Lond. Ser. A Math. Phys. **274(1356)**, 21–39 (1963)

[32] Thimons, L.A., Gujrati, A., Sanner, A., Pastewka, L., Jacobs, T.D.: Hard-material adhesion: Which scales of roughness matter? Experimental Mechanics **61**(7), 1109–1120 (2021)

[33] Persson, B.N., Scaraggi, M.: Theory of adhesion: Role of surface roughness. The Journal of chemical physics **141**(12) (2014)

[34] Violano, G., Demelio, G.P., Afferrante, L.: On the dmt adhesion theory: from the first studies to the modern applications in rough contacts. Procedia Structural Integrity **12**, 58–70 (2018)

[35] Tabor, D.: Surface forces and surface interactions. In: Plenary and Invited Lectures, pp. 3–14. Elsevier, ??? (1977)

[36] Van Dokkum, J.S., Pérez-Rafols, F., Dorogin, L., Nicola, L.: On the retraction of an adhesive cylindrical indenter from a viscoelastic substrate. Tribology International **164**, 107234 (2021)

[37] Afferrante, L., Violano, G.: On the effective surface energy in viscoelastic hertzian contacts. Journal of the Mechanics and Physics of Solids **158**, 104669 (2022)

[38] Müser, M.H., Persson, B.N.: Crack and pull-off dynamics of adhesive, viscoelastic solids. Europhysics Letters **137**(3), 36004 (2022)

[39] Papangelo, A., Ciavarella, M.: Detachment of a rigid flat punch from a viscoelastic material. Tribology letters **71**(2), 48 (2023)

[40] Mandriota, C., Menga, N., Carbone, G.: Adhesive contact mechanics of viscoelastic materials. International Journal of Solids and Structures **290**, 112685 (2024)

[41] Papangelo, A., Nazari, R., Ciavarella, M.: Friction for a sliding adhesive viscoelastic cylinder: Effect of maugis parameter. European Journal of Mechanics-A/Solids, 105348 (2024)

[42] Afferrante, L., Violano, G., Demelio, G.P.: Sliding viscoelastic contacts: The role of adhesion, boundary conditions, and finite geometry. Tribology Letters **73**, 5 (2025)

[43] Clerk Maxwell, J.: On the dynamical theory of gases. Philosophical Transactions of the Royal Society of London Series I **157**, 49–88 (1867)

[44] Derjaguin, B.: Untersuchungen ueber die reibung und adhaesion, iv: Theorie des anhaftens kleiner teilchen. Kolloid-Zeitschrift **69**, 155–164 (1934)

[45] Yu, N., Polycarpou, A.A.: Adhesive contact based on the lennard–jones potential: a correction to the value of the equilibrium distance as used in the potential. Journal of Colloid and Interface Science **278**(2), 428–435 (2004)

[46] Greenwood, J.: Adhesion of elastic spheres. Proceedings of the Royal Society of London. Series A: Mathematical, Physical and Engineering Sciences **453**(1961), 1277–1297 (1997)

[47] Feng, J.Q.: Contact behavior of spherical elastic particles: a computational study of particle adhesion and deformations. Colloids and Surfaces A: Physicochemical and Engineering Aspects **172**(1-3), 175–198 (2000)

[48] Feng, J.Q.: Adhesive contact of elastically deformable spheres: a computational study of pull-off force and contact radius. Journal of colloid and interface science **238**(2), 318–323 (2001)

[49] Persson, B.N.: Theory of rubber friction and contact mechanics. The Journal of Chemical Physics **115**(8), 3840–3861 (2001)

[50] Carbone, G., Putignano, C.: A novel methodology to predict sliding and rolling friction of viscoelastic materials: Theory and experiments. Journal of the Mechanics and Physics of Solids **61**(8), 1822–1834 (2013)